Adiabatic heating and convection caused by a fixed-heat-flux source in a near-critical fluid

E. B. Soboleva*

Institute for Problems in Mechanics, Russian Academy of Sciences, Prospect Vernadskogo, 101, b.1, 119526 Moscow, Russia

(Received 1 August 2002; revised manuscript received 11 July 2003; published 1 October 2003)

Dynamics and heat transfer in a near-critical fluid in a square cavity with a finite heat source located at the bottom are studied numerically. A thermally insulated enclosure and a fixed-heat-flux source are considered. The two-dimensional simulation is based on the full Navier-Stokes equations with two-scale splitting of the pressure and the van der Waals equation of state. It is shown that the piston effect is independent of convection. Near the critical point, this effect becomes independent of criticality and convective motions are damped.

DOI: 10.1103/PhysRevE.68.042201 PACS number(s): 65.20.+w, 47.11.+j, 05.70.Jk, 47.15.−x

Media with parameters close to the thermodynamic critical point display specific physical properties [1]. They are characterized by some coefficients which, with approach to the critical point, grow unboundedly (specific heat at constant pressure and compressibility) or vanish (thermal conductivity). More than 10 years ago, it was revealed that a heat source inside a near-critical fluid can cause rapid thermalization of a bulk fluid. This effect, called the ''piston effect'' (PE) was observed experimentally [2,3] and explained theoretically [4–6]. The PE is associated with an expansion-compression mechanism. When a source emits heat, the thermal boundary layer formed nearby expands strongly and pushes the bulk fluid as a piston. This leads to compression and adiabatic thermalization of the bulk fluid. This heating mechanism was studied for one-dimensional (1D) geometry and temperature-step source [4–6] and other sources in thermostated containers [5,6]. The role of boundary effects was discussed in Ref. [7]. In real configurations, an interplay between the PE and thermal gravity–driven convection may occur. The 2D simulations were performed to study the hydrodynamic stability in the Rayleigh-Bénard configuration [8,9], transport phenomena in a side-heated cavity [10], convective jet motions under terrestrial [11] and nonuniform microgravity [12] conditions. It was revealed [10,11] that convection can enhance the PE thermalization induced by a constant-temperature source. However, it was not discussed whether this effect is universal or it occurs only in some conditions. Internal sources of constant power contained in thermostated or partially thermostated enclosures were investigated in Refs. [11,12]. In those cases, heat fluxes from the boundaries disturbed the thermal field inside. In this paper, a fixed-heat-flux source in a container with adiabatic walls is considered to realize the fluid response to a localized steady heat supply. We present the results of numerical simulations both in terrestrial and in zero-gravity conditions and discuss the distinctions from the results obtained earlier for a step-temperature source.

The hydrodynamic model applied here consists of the full Navier-Stokes equations and the energy equation for a nonperfect compressible medium with an arbitrary two-parameter equation of state. The pressure is decomposed into two components: a volume-average part and a dynamic part [13]. To close the set of equations, the integral balance of the dynamic pressure component is added. The governing equations may be written in dimensionless form as follows:

$$\frac{\partial \rho}{\partial t} + \vec{\nabla}\cdot(\rho \vec{U}) = 0, \tag{1}$$

$$\rho \frac{\partial \vec{U}}{\partial t} + \rho(\vec{U}\cdot\vec{\nabla})\vec{U} = -\vec{\nabla}p + \frac{1}{\mathrm{Re}}\left[2\vec{\nabla}\cdot(\eta \mathrm{D}) - \vec{\nabla}\left(\frac{2}{3}\eta - \varsigma\right)(\vec{\nabla}\cdot\vec{U})\right] + \frac{1}{\mathrm{Fr}}\rho\vec{g}, \tag{2}$$

$$\rho \frac{\partial T}{\partial t} + \rho(\vec{U}\cdot\vec{\nabla})T = -(\gamma_0 - 1)T\left(\frac{\partial P}{\partial T}\right)_\rho (\vec{\nabla}\cdot\vec{U}) + \frac{\gamma_0}{\mathrm{Re\,Pr}}\vec{\nabla}\cdot(\lambda\vec{\nabla}T) + \frac{\gamma_0(\gamma_0-1)M^2}{\mathrm{Re}} \times \left[2\eta \mathrm{D}^2 - \vec{\nabla}\left(\frac{2}{3}\eta - \varsigma\right)(\vec{\nabla}\cdot\vec{U})^2\right], \tag{3}$$

$$P = P(\rho, T), \tag{4}$$

$$P = \langle P\rangle + \gamma_0 M^2 p, \quad \int_V p\,dv = 0. \tag{5}$$

Here ρ, $\vec{U}$, D, T are the density, velocity, strain rate tensor, and temperature; P, $\langle P\rangle$, and p are the total pressure, the volume-average, and dynamic pressure components; $\vec{g}$ is the mass force acceleration; η, ς, λ are the dynamic viscosity, bulk viscosity, and heat conductivity; dv is an elementary volume; and V is the overall volume. The characteristic scales are the following: length l', velocity u', time l'/u', strain rate u'/l', Earth's gravity force acceleration g', the critical values (denoted by the subscript ''c'') ρ_c', T_c', and the values λ_0', η_0', c_{v0}' corresponding to a perfect gas (denoted by the subscript ''0''). The dimensional values are indicated by a prime while the nondimensional values have no prime.

The set of equations includes the Reynolds, Froude, Prandtl, Mach numbers, and the ratio of specific heats for a perfect gas, which are defined as

*Email address: soboleva@ipmnet.ru;
URL: http://www.ipmnet.ru/~soboleva

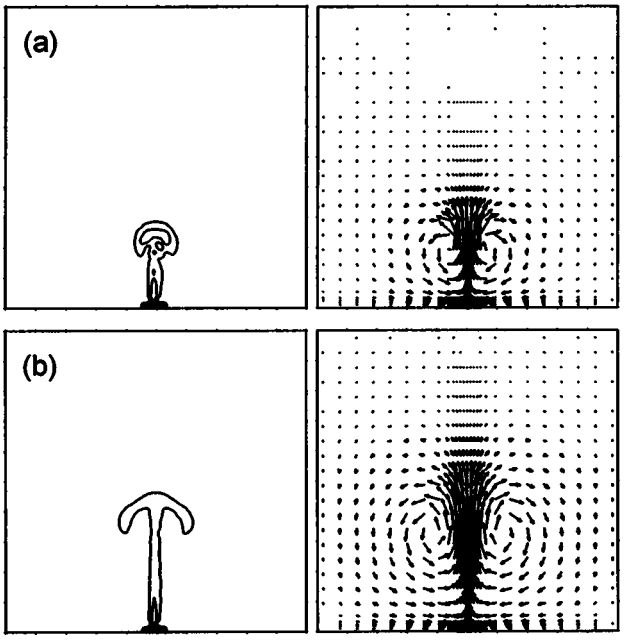

FIG. 1. Isotherms and dynamic fields at the instants $t'=5.0$ (a) and 7.6 s (b).

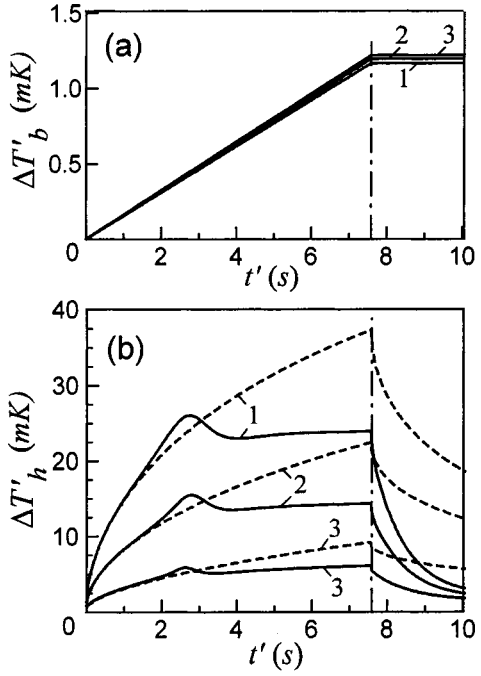

FIG. 2. Time dependencies of $\Delta T'_b$ (a) and $\Delta T'_h$ (b) at $\varepsilon=1.64\times10^{-2}$ (1), 6.58×10^{-3} (2), 1.64×10^{-3} (3) in the terrestrial environment (continuous curves). Broken curves (b) correspond to zero gravity. Dot-and-dash vertical line indicates the instant when the source is switched off.

$$\mathrm{Re}=\frac{\rho'_c u' l'}{\eta'_0},\quad \mathrm{Fr}=\frac{u'^2}{g'_0 l'},\quad \mathrm{Pr}=\frac{(c'_{v0}+B')\,\eta'_0}{\lambda'_0},$$

$$M=\frac{u'}{\sqrt{\gamma_0 B' T'_c}},\quad \gamma_0=1+\frac{B'}{c'_{v0}}. \tag{6}$$

Here, $B'=R'/\mu'_g$, R' is the perfect gas constant, and μ'_g is the molar mass.

For modeling near-critical fluids, we will use the van der Waals equation of state

$$P=\rho T/(1-b\rho)-a\rho^2,\quad a=9/8,\quad b=1/3. \tag{7}$$

The coefficient λ increases on approaching the critical point as $\lambda=1+\Lambda[(T'-T'_c)/T'_c]^{-\psi}$ [1], η is assumed to be constant, and ς is equal to zero. The fluid is stratified. The density and pressure variations along the body force vector are described at the initial instant by the linear relations [14].

The total pressure P in the governing equations is decomposed into two parts (the volume-average pressure $\langle P\rangle$ and the dynamic pressure p). These parts are normalized using the different scales ($B'\rho'_c T'_c$ for $\langle P\rangle$ and $\rho'_c U'^2$ for p). In the limit of small Mach numbers this model approaches the acoustic-filtering model [15] and may be successfully applied for simulating a low-speed dynamics with a large time step. However, the present model describes acoustic processes as well since we do not remove p from P in the equation of state.

A 2D numerical solver based on a finite-difference formulation has been designed. The space discretization on a straggled grid using second-order implicit schemes is employed. Nonuniform rectangular grids are used. The procedure is split into several steps. The volume-average pressure $\langle P\rangle$ and density ρ are calculated by an iterative method from the equation of state and Eq. (5). Then, Eqs. (1) and (2) are integrated by the SIMPLE-type algorithm [16], and the density, velocity, and dynamic pressure are corrected successively according to requirements on conservation. After that, the magnitudes of p are shifted and $\langle P\rangle$ is recalculated to satisfy Eq. (5). Finally, Eq. (3) is integrated yielding the magnitude of T. To ensure a high calculation accuracy, the governing equations were rewritten in reduced variables $\delta f=f-f_c$, where $f=(\rho,\langle P\rangle,p,T)$ and Eqs. (2) and (3) were transformed into conservative form.

The present numerical code was applied to simulations of heat transfer in enclosures with side heating and cooling [17]. This code was modified as compared to the earlier version based on the acoustic-filtering model. Using the previous version of the code, we studied the problems of convective motions in near-critical fluids in microgravity [18] and terrestrial conditions [14] and examined the role of the equation of state [19].

The thermally insulated square cavity filled with a near-critical CO_2 under terrestrial conditions is considered. A source of energy is located very close to the center of the lower surface and one can assume that it stands at the bottom. The side of the cavity is $l'=1$ cm and the length of the heater is $h'=0.06$ cm. Initially, the velocity is zero, the temperature is constant, and the density at the top boundary is critical. At the initial instant, the fixed-power source with the heat flux $q'=0.582$ mW/cm^2 is switched on and it operates during a time internal $t'_h=7.6$ s. The dimensionless parameters are $\mathrm{Re}=3.85\times10^4$, $\mathrm{Pr}=1.0$, $M=10^{-3}$, $\gamma_0=1.4$, $\mathrm{Fr}=0.820$, and $\vec{g}=(0,-1)$ for the velocity scale to be u'

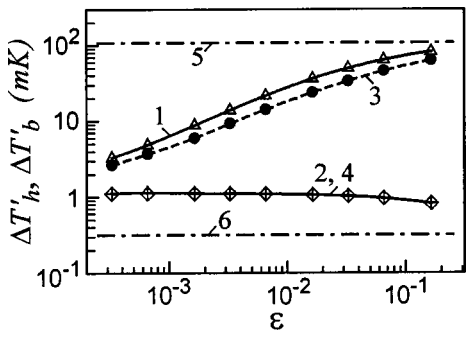

FIG. 3. The values $\Delta T'_h$ and $\Delta T'_b$ vs ε for a near-critical fluid (NCF) and a perfect gas (PG) in the terrestrial $[\vec{g}=(0,-1)]$ and zero-gravity $(\vec{g}=0)$ environments at the instant $t'=7.0$. Line 1: $\Delta T'_h$, NCF, $\vec{g}=0$; 2: $\Delta T'_b$, NCF, $\vec{g}=0$; 3: $\Delta T'_h$, NCF, $\vec{g}=(0,-1)$; 4: $\Delta T'_b$, NCF, $\vec{g}=(0,-1)$; 5: $\Delta T'_h$, PG, $\vec{g}=0$; 6: $\Delta T'_b$, PG, $\vec{g}=0$. Marks denote the calculated points.

$=28.5$ cm/s. The coefficient λ is determined from the experimental data [20] yielding the constants $\Lambda=0.028$ and $\psi=0.74$. The reduced temperature $\varepsilon=(T'_i-T'_c)/T'_c$ (where T'_i is the initial temperature) varied in the calculations.

The calculation accuracy was controlled by checking the overall balances of internal energy and kinetic energy. The deviations in the first balance were less than 0.5% and in the second one less than 1–2 %. The typical integration was performed on a 81×101 grid with the grid-point clustering near the source (the cluster coefficients were equal to 5.0 and 6.7). The minimum spatial step was $h_{\min}=1.83\times10^{-3}$. The time step Δt was determined from the formula $\Delta t=\mathrm{Ku}\, h_{\min} M$ (where Ku is the Courant number) for $\mathrm{Ku}=9.07\times10^2$.

As is known, a source of energy induces global heating by the PE mechanism and convection [10–12,14,17]. The typical pattern in the present configuration obtained at $\varepsilon=6.58\times10^{-3}$ (initial temperature was 2 K above the critical point) is shown in Fig. 1. It is clear that the upward convective jet rises from the source. A maximum velocity modulus has a magnitude $|\vec{U}'|_{\max}=0.154$ cm/s at the instant $t'=5.0$ s and $|\vec{U}'|_{\max}=0.172$ cm/s at $t'=7.6$ s.

The values of the relative temperature $\Delta T'=T'-T'_i$ at the source center and at the center of the top boundary are denoted as $\Delta T'_h$ and $\Delta T'_b$. In some simulations, the body force is "switched off," hence, convection is canceled. Under weightlessness conditions, the $\Delta T'_b$ functions increase linearly if the source is active and are constant if it is switched off [Fig. 2(a)]. Since the increment in $\Delta T'_b$ characterizes the intensity of the PE, one can see that the PE characteristic time is equal to t'_h and ε has only slight influence on the thermalization rate. This situation is different from that governed by a step-temperature source which leads to a shorter PE time scale and stronger thermalization with approach to the critical point [4–6]. In that consideration, the amount of heat entering the fluid is not limited and determined by the fluid compressibility enhanced as $\varepsilon\to0$. However, if the heat flux is fixed, as here, the fluid cannot absorb more energy than it is supplied and the rate of the PE temperature increase is limited. When the source is switched off,

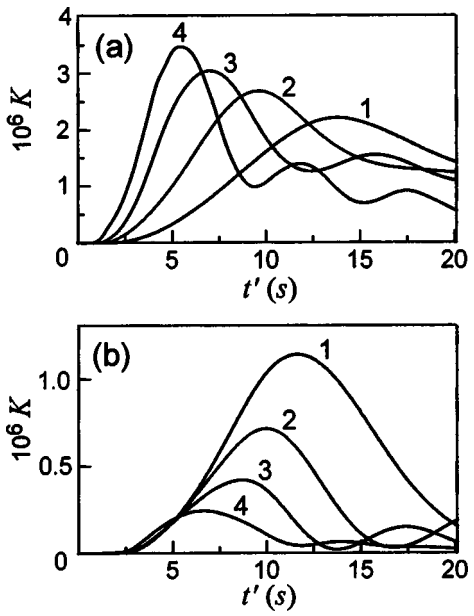

FIG. 4. Time dependence of K for the cases of the fixed-temperature source at the initial temperature step of 20 mK (a) and fixed-heat-flux source (b) at $\varepsilon=1.64\times10^{-2}$ (1), 6.58×10^{-3} (2), 3.29×10^{-3} (3), and 1.64×10^{-3} (4).

the PE stops. The value $\Delta T'_h$ [Fig. 2(b)] characterizing the thermal inhomogeneity near the source rises with time for $t'<t'_h$. However, when $\varepsilon\to0$, $\Delta T'_h$ increases much slower, i.e., the thermal energy is removed from the boundary layer and transformed into the bulk heat more intensively.

Under terrestrial conditions, the $\Delta T'_b$ functions at all ε considered remain the same as for zero gravity, accordingly, we did not plot them in Fig. 2(a). Convection does not change the intensity of the PE that is opposite to the case of a step-temperature source when convection can enhance the PE [10,11]. However, the temperature of the source, $\Delta T'_h$, decreases in Fig. 2(b) since cold streams flow past the source and cool it.

The variations of ε in a wide range demonstrated (Fig. 3) that, far from the critical point, a substantial portion of energy is accumulated in the boundary layer. This results in large magnitudes of $\Delta T'_h$ and magnitudes of $\Delta T'_b$ which are smaller than limiting value. As $\varepsilon\to0$, the difference between $\Delta T'_h$ and $\Delta T'_b$ vanishes. Convection results in additional reduction of $\Delta T'_h$. A medium at near-critical parameters does not allow the source temperature to rise significantly, therefore it can be considered as an effective cooler.

To analyze the effect of the PE on convection, we will estimate the dimensionless kinetic energy of the whole fluid, $K=0.5\int_V \rho(t)\vec{U}^2(t)dv$, associated with convective motions. The present problem is compared with the problem for the fixed-temperature source, other things being identical. In the second case, as shown in Fig. 4(a), the convective flow becomes more intense as $\varepsilon\to0$. On the contrary, in the first case, the intensity of convection decreases as $\varepsilon\to0$ [Fig. 4(b)]. As discussed above, thermalization in this case tends

to the spatially uniform distribution of temperature with a small thermal inhomogeneity near the source and, hence, convective jets are weaker. We may assume that with the further decrease in ε, convection will be completely damped. This will make it possible to distinguish the PE mechanism even in the presence of gravity.

In summary, it should be noted that the present numerical study can match experimental results with some precautions. The van der Waals equation of state does not ensure a high accuracy in description of real near-critical fluids, especially, in a close vicinity of the critical point. We do not take 3D effects into account and do not investigate the effects of real geometry. Nevertheless, the present consideration shows that limited heat fluxes from the source lead to some universal features in near-critical dynamics and heat transfer. Global thermalization in this case is independent of convective motions. With approach to the critical point, it becomes independent of criticality and convection becomes weaker.

The author is indebted to Professor V. I. Polezhaev for his idea to investigate effects of heaters and boundary conditions on near-critical heat transfer and for helpful discussions, and Dr. M. K. Ermakov for the interest in this study. The work received financial support from the Russian Foundation for Basic Research (Grant Nos. 00-01-00401 and 03-01-00682).

[1] H. E. Stanley, *Introduction to Phase Transition and Critical Phenomena* (Oxford Science, New York, 1987).
[2] K. Nitsche and J. Straub, Naturwissenschaften **73**, 370 (1986).
[3] D. Beysens *et al.*, in *Fluid Science & Material Science in Space*, edited by H. U. Walter (Springer-Verlag, Paris, 1987), p. 221.
[4] A. Onuki *et al.*, Phys. Rev. A **41**, 2256 (1990).
[5] B. Zappoli and A. Durand-Daubin, Phys. Fluids **6**, 1929 (1994).
[6] B. Zappoli and P. Carlès, Eur. J. Mech. B/Fluids **14**, 41 (1995).
[7] A. Jounet *et al.*, Phys. Rev. Lett. **84**, 3224 (2000).
[8] S. Amiroudine *et al.*, J. Fluid Mech. **442**, 119 (2001).
[9] A. Furukawa and A. Onuki, Phys. Rev. E **66**, 016302 (2002).
[10] B. Zappoli *et al.*, J. Fluid Mech. **316**, 53 (1996).
[11] B. Zappoli *et al.*, J. Fluid Mech. **388**, 389 (1999).
[12] A. Jounet, Phys. Rev. E **65**, 037301 (2002).
[13] A. G. Churbanov *et al.*, in *Proceedings of the Tenth International Conference on Numerical Methods in Laminar and Turbulent Flow, Swansea, 1997*, edited by C. Taylor (Pineridge Press, Swansea, 1997).
[14] V. I. Polezhaev and E. B. Soboleva, Izv. Akad. Nauk, Mekh. Zhidk. Gasa **3**, 143 (2001) [Fluid Dyn. **36**, 467 (2001)].
[15] S. Paolucci, Report No. SAND 82-8257, 1982 (unpublished).
[16] S. V. Patankar, *Numerical Heat Transfer and Fluid Flow. Computational Methods in Mechanics and Thermal Science* (Hemisphere, New York, 1980).
[17] V. I. Polezhaev and E. B. Soboleva, Izv. Akad. Nauk, Mekh. Zhidk. Gasa **1**, 81 (2002) [Fluid Dyn. **37**, 72 (2002)].
[18] V. I. Polezhaev and E. B. Soboleva, Izv. Akad. Nauk, Mekh. Zhidk. Gasa **3**, 70 (2000) [Fluid Dyn. **35**, 371 (2000)].
[19] E. B. Soboleva, Teplofiz. Vys. Temp. **38**, 928 (2000) [High Temp. **38**, 893 (2000)].
[20] J. V. Sengers, in *Transport Phenomena—1973*, edited by J. Kestin, AIP Conf. Proc. No. **11** (AIP, New York, 1973).